Accepted Manuscript online: 2022-07-27 Article published online: 2022-09-15

Copper-Templated Formation of Dihelical Oligothiophene–Phenanthroline Assemblies

Sylvia Schmid *[a]
Markus Wunderlin[a]
Elena Mena-Osteritz[a]
Peter Bäuerle *[a]

[a] Institute of Organic Chemistry II, University of Ulm, Albert-Einstein-Allee 11, D-89081 Ulm, Germany
* sylvia.schmid@uni-ulm.de; peter.baeuerle@uni-ulm.de

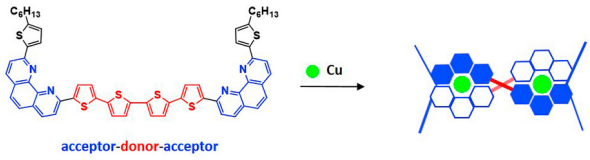

Received: 20.06.2022
Accepted after revision: 21.07.2022
DOI: 10.1055/a-1910-9165; Art ID: OM-2022-06-0009-OA

Abstract We report the synthesis and comprehensive characterization of a series of (oligo)thiophene-bridged (bis)phenanthroline ligands. The complexation behavior of the ditopic ligands with Cu(I) was explored by high-resolution ESI mass spectrometry, UV-vis spectroscopy, and electrochemistry. Whereas ligands, in which the phenanthrolines are bridged by smaller (oligo)thiophene units, provided mainly mononuclear complexes, quaterthiophene-based ditopic ligands show a strong tendency to undergo metal-templated self-assembly into double-stranded, dinuclear helicates.

Key words: oligothiophenes, phenanthrolines, helicates, copper(I) complexation, optoelectronic properties

Introduction

Oligothiophenes (OTs) represent π-conjugated organic semiconductors[1] for versatile applications in electronic devices, such as organic field effect transistors,[2] organic light-emitting diodes,[3] or organic solar cells.[4] Covalent linkage of the electron-donating (D) OTs to electron-withdrawing acceptor (A) groups opens prospects to modulate the photophysical and electrochemical properties of redox active A–D systems by variation of the overall length of the π-conjugated scaffolds.[5] Implementation of N-heterocyclic 1,10-phenanthrolines (*phen*) into D–A molecules enables the development of fully π-conjugated ligands with coordinative binding sites for N-protonation or chelation to transition metals.[6,7] Hence, numerous *phen* ligands have been reported as suitable materials for cation or anion sensing allowing for potential utilization as environmental and biological probes.[8] The excellent chelation properties of *phen*-based ligands towards transition metal complexes have raised strong interest and various bis-*phen* metal complexes found applications in organic light-emitting diodes[9] or as redox mediators in dye-sensitized solar cells.[10,11] In addition, *phen*-based ligands were utilized to synthesize via metal-template strategies sophisticated functional molecular architectures such as supramolecular racks and baskets,[12] interlocked molecular structures like catenanes,[13] or (pseudo) rotaxanes.[14–17] Particularly, for the synthesis of molecular knots, preorganization of two ditopic (bis-chelating) ligands into double-stranded helicates around two Cu(I) ions is required.[18–21]

More recently, strong interest emerged for applications of multinuclear transition metal complexes[22] in photosensitized water splitting.[23,24] The presence of π-conjugated bridging segments such as OTs between two metal chelating sites introduces potential for enhanced metal–metal coupling allowing for potential application as switchable devices in molecular electronics.[25,26] The majority of devices developed so far are based on ruthenium polypyridyl derivatives[27,28]; however, copper complexes of 2,9-arylated *phens* showed favorable photophysical properties.[29,30] Replacement of less abundant ruthenium by copper was considered to be a less expensive alternative. In addition, compared to more flexible ter- and bipyridines, which often lack directionality in their coordination behavior, *phens* should be superior because the angle between the two chelation moieties is fixed.[12b]

We now aimed at the development of a series of symmetric, A–D–A-type, ditopic (oligo)thiophene-*phen* ligands, which self-organize via metal-templation into a double-stranded helicate. Generation of two or more metal centers connected via a rigid, π-conjugated bridge should enable the development of new functional topologies with defined spatial distribution. In various examples it has been shown that appropriate functionalization of linear OTs with polar moieties such as peptides[31–33] or poly(ethylene oxide)[34] promotes the formation of supramolecular nanostructures. Metal-assisted organization of symmetric OT-*phen*-based ligands into a dimeric dihelical arrangement should benefit from intermolecular π–π stacking interactions of the linear OT-linkers on one hand and from the preference of spherical d^{10}-Cu(I) ions to adopt a pseudotetrahedral (D_{2d}) coordina-

tion with α,α′-diamine ligands such as *phen* on the other hand.

In this communication, we now report synthesis and optoelectronic characterization of a series of (oligo)thiophene-bridged bis-phenanthroline ligands **L1**–**L4** and hexyl-substituted quaterthiophene derivative **L4′**. The coordination behavior of the ligands towards Cu(I) was explored via ESI-HRMS, ^{1}H-NMR spectroscopy, and optical and electrochemical measurements which enabled the identification of suitable ligands for the generation of dimeric Cu(I) complexes with a dinuclear configuration.

Results and discussion

(Oligo)thiophene-bridged bis-phenanthroline ligands L1–L4 and L4′

Synthesis

The synthetic route to thiophene (1 T)-bridged bis-phenanthroline ligand **L1** starts with a Suzuki-type cross-coupling reaction of 2-hexyl-5-thienyl boronic acid pinacol ester **1** and 2,9-dichloro-1,10-phenanthroline **2**, which afforded 2-hexylthiophene-substituted phenanthroline **3** in 68% yield (Scheme 1). Subsequently, the thienylated *phen* derivative **3** was used as a starting material for a twofold Stille cross-coupling reaction with *bis*-stannylated thiophene **4**, from which the symmetrical 1 T-bridged ligand **L1** was isolated in 78% yield. Synthesis of bithiophene (2 T)-based ligand **L2** and dihexyl-quaterthiophene (4 T)-bridged ligand **L4′** were feasible applying the same synthetic strategy. Both representatives were accessible in acceptable yields of 68% (**L2**) and 63% (**L4′**) from Stille-type cross-coupling reaction of thienylated phenanthroline **3** and *bis*-stannylated building blocks **5** or **6**, respectively.

Syntheses of terthiophene (3 T) and quaterthiophene (4 T)-bridged bis-*phen* ligands **L3** and **L4** were carried out differently (Scheme 2). For the preparation of ligand **L3,** chloro derivative **3** was converted into the more reactive iodinated **8** by nucleophilic substitution with sodium iodide. Subsequent Stille-type cross-coupling reaction of iodinated *phen* **8** and *bis*-stannylated terthiophene **7** afforded ligand **L3** in 71% yield.

A Suzuki-type cross-coupling reaction of 2,9-dichloro-*phen* **2** with bithiophene pinacol boronic ester **9**[35] delivered monosubstituted *phen* **10** in 62% yield, which was further coupled with 2-hexylthiophene pinacol boronic ester **1** under Pd-catalysis in order to obtain unsymmetrical 2,9-arylated *phen* **11** in 80% yield. The following halogenation of **11** with *N*-iodosuccinimide (NIS) at the free α-position of

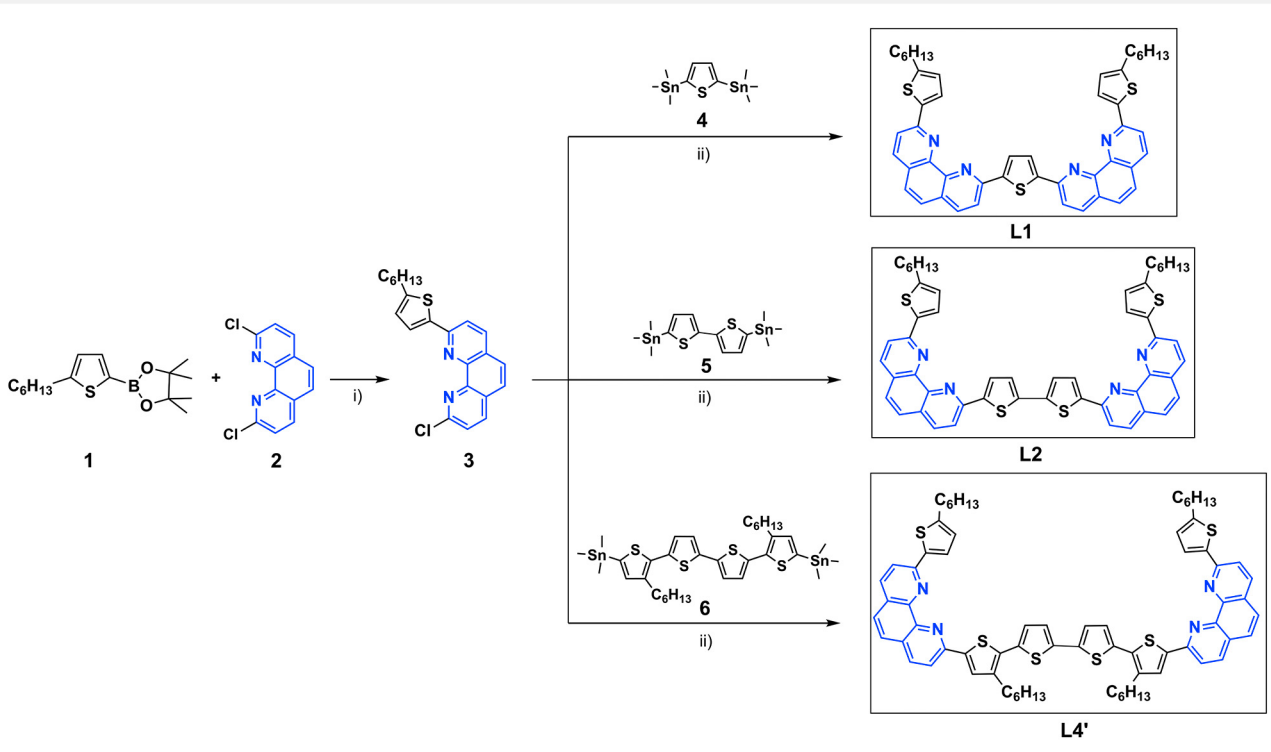

Scheme 1 Synthetic pathway to phenanthroline-(oligo)thiophene ligands **L1**, **L2**, and **L4′**. (i) $Pd[PPh_3]_4$, Cs_2CO_3, DME : H_2O (4 : 1), 80 °C, 16 h, 68% yield; (ii) $Pd[PPh_3]_4$, toluene, 100 °C, 16 h, 78% yield (**L1**), 68% yield (**L2**), 63% yield (**L4′**).

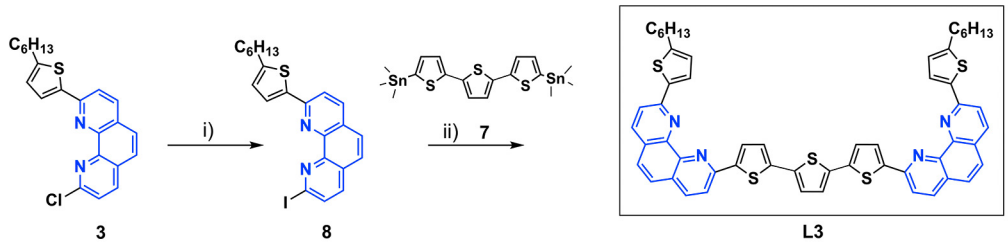

Scheme 2 Synthesis of ligand **L3:** (i) HI, H_3PO_2, NaI, 93 °C, 1 h, 84% yield; (ii) $Pd[PPh_3]_4$, toluene, 100 °C, 16 h, 71% yield.

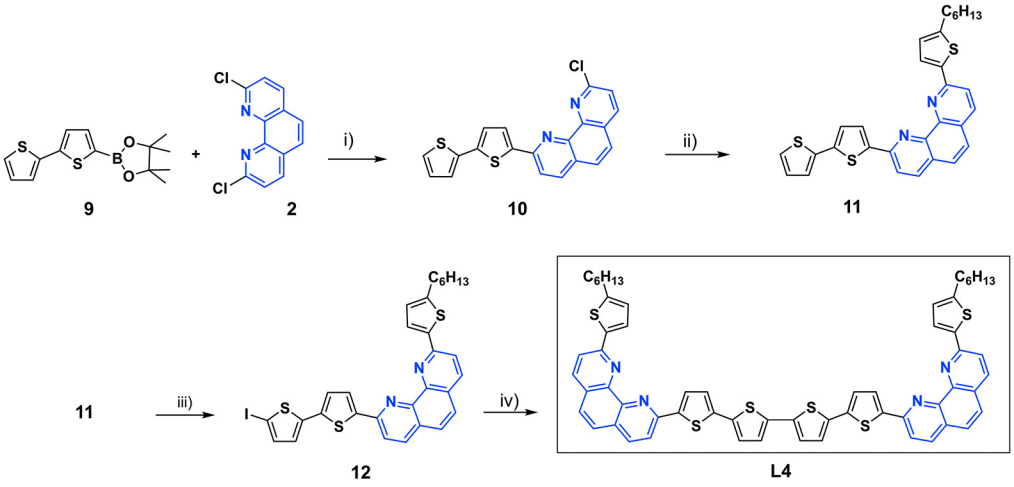

Scheme 3 Synthetic pathway to phenanthroline-quaterthiophene ligand **L4.** (i) $Pd[PPh_3]_4$, $Ba(OH)_2 \cdot 8\ H_2O$, DME/H_2O (4:1), 80 °C, 16 h, 62% yield; (ii) 2-hexyl-5-thienyl boronic acid pinacol ester **1**, $Pd[PPh_3]_4$, Na_2CO_3, dioxane, 80 °C, 16 h, 80% yield; (iii) NIS, $CHCl_3$:DCM (1:1), CH_3COOH (cat.), 87% yield; (iv) B_2pin_2, $Pd(dppf)Cl_2 \cdot CH_2Cl_2$, $K^+CH_3COO^-$, dioxane, 71% yield.

the bithiophene unit gave access to iodinated derivative **12** in 87% yield. Finally, symmetric 4 T-bridged bis-*phen* ligand **L4** was accessible by homocoupling of halogenated **12** in the presence of bis(pinacolato)diborane (B_2pin_2) in 71% yield (Scheme 3). The structures of all novel derivatives were investigated and evidenced by ^{1}H- and ^{13}C-NMR spectroscopy and MALDI-HRMS (Figures S1–S20, Supporting Information).

Optical properties

Since ligands **L2** and **L4** were sparely soluble in dichloromethane (DCM), tetrahydrofuran (THF) was used as the solvent for the optical characterization of all free ligands (Figure 1, left; Table 1). The absorption spectra of the ligands **L1**–**L4** and **L4′** revealed characteristics of multichromophoric systems with various absorption bands corresponding to different electronic transitions. Among them, for all derivatives the low-energy band can be ascribed to a π–π* transition (red filled curve in Figure 1, left, top), which is continuously bathochromically shifted from 400 to 454 nm with increasing π-conjugation of the (oligo)thiophene bridge for **L1** to **L4**. Accordingly, the energy gap diminishes from 2.81 to 2.35 eV. In the case of **L1** a pronounced vibronic fine structure of the low-energy band can be observed which indicates coplanarity of the individual *phen* and thiophene subunits. The fine structure gradually disappears on going to the larger ligands **L4** and **L4′** due to increasing torsional flexibility of the thiophene rings in the bridge. Despite the 4 T-based ligands **L4** and **L4′** comprise identical chromophores, the low-energy band of ligand **L4′** is hypsochromically shifted by 14 nm compared to **L4** mostly due to a more twisted conformation of the 4 T-bridge caused by the hexyl side chains. The strong absorption in the regime of 280–400 nm can be addressed to *phen* units (green filled curve in Figure 1, left, top) in accordance with the literature data on phenylated[36–38] and thiophene-substituted *phens*[13b] and

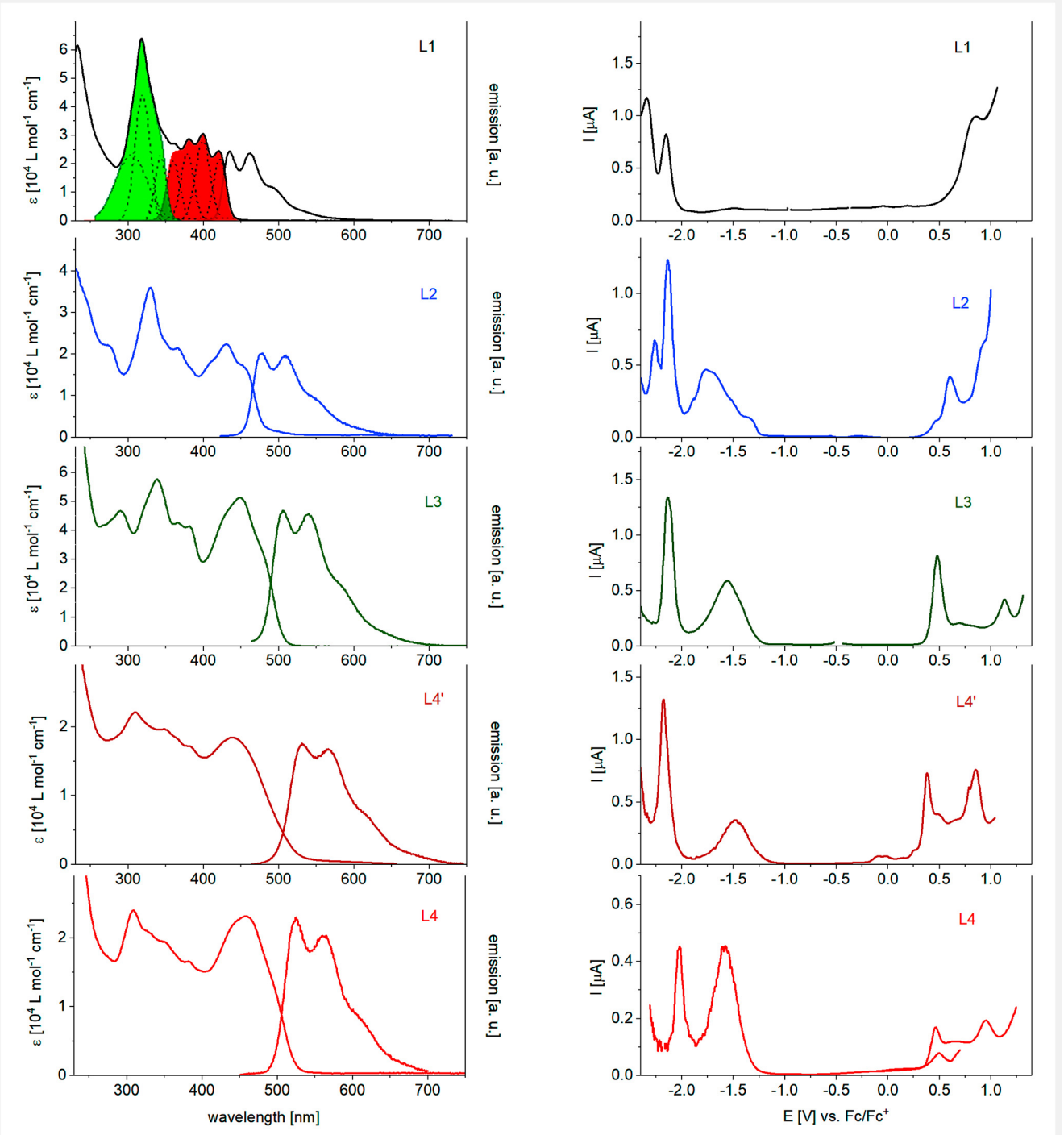

Figure 1 UV-vis ($c = 10^{-5}$ M) and fluorescence spectra ($c = 10^{-8}$ M, λ_{exc} 360 nm) of **L1**–**L4** and **L4′** measured in THF (left); inset in UV-vis spectrum of **L1** (black line): the mathematically deconvoluted Gaussian curves (dotted lines). The sum of the four first deconvoluted curves (filled red curve) corresponds to the contribution in the absorption spectrum of the long axis π–π* electronic transition. The filled green curve consists of the sum of three deconvoluted Gaussian curves and mainly corresponds to the absorption of the *phen* units. Differential pulse voltammograms of **L1**–**L4** and **L4′** measured in DCM/tetrabutylammonium hexafluorophosphate (0.1 M) versus ferrocene/ferricenium (Fc/Fc^+), 100 mV/s, r.t. (right).

Table 1 Optical and electrochemical data of ligands **L1**–**L4** and **L4′**. Absorption and emission spectra were measured in THF at room temperature, maxima are underlined.

Ligand	λ_{max}^{abs} [nm]	ε [$M^{-1} \cdot cm^{-1}$]	λ_{onset} [nm]	E_g^{opt} [eV]	λ_{max}^{em} [nm]	$E_{1/2}^{Ox1}$ [V]	$E_{1/2}^{Ox2}$ [V]	$E_{1/2}^{Red1}$ [V]	$E_{1/2}^{Red2}$ [V]	E_g^{CV} [eV]
L1	318, 400	66 180	438	2.81	435, 461	1.00	–	−2.00	−2.15	2.71
L2	332, 432	36 500	482	2.57	478, 509	0.61	–	−1.75	−2.15	1.63
L3	338, 446	57 250	508	2.44	507, 540	0.45	0.76	−1.80	−1.90	1.56
L4	312, 452	24 000	527	2.35	524, 561	0.31	0.68	−1.70	−2.01	1.42
L4′	310, 440	22 000	522	2.38	531, 566	0.38	0.74	−1.69	−2.23	1.43

E_g^{opt} calculated with $1240/\lambda_{onset}$. CV in DCM/tetrabutylammonium hexafluorophosphate (0.1 M), 100 mV · s^{-1}, r. t., potentials referenced against Fc/Fc^+. E_g^{CV} calculated by the difference of the first oxidation and reduction onset potentials.

as a minor contribution to low-intensity n–π^* transitions, which should also appear in this region. The emission spectra of ligands **L1**–**L4** and **L4′** showed fine-structured bands, coherent with a mostly coplanar structure of the emitting excited state, and undergo bathochromic shifts from 461 to 531 nm with increasing π-conjugation.

Electrochemical properties

In order to get information about the redox properties, (oligo)thiophene-bis-*phen* ligands **L1**–**L4** and **L4′** were studied by cyclic voltammetry (CV) and differential pulse voltammetry (DPV) using DCM or THF as the solvent and tetrabutylammonium hexafluorophosphate ($TBAPF_6$ 0.1 M) as the conducting salt. All potentials were referenced against the ferrocene/ferricenium couple (Fc/Fc^+) and data are compiled in Table 1. DPVs of the ligands measured in DCM are depicted in Figure 1 (right). As a general trend, it was found that with increasing length of the (oligo)thiophene bridge, the oxidation potential ($E_{1/2}^{Ox1}$) is progressively negatively shifted from 1.0 to 0.31 V, reflecting the typical formation of (oligo)thiophene radical cations. Furthermore, for the longer derivatives **L4** and **L4′** a second oxidation wave ($E_{1/2}^{Ox2}$) concomitant with the formation of dications at around 0.7 V is noticed.[3,39] In the reductive potential regime, reduction of the *phen* unit(s) to radical anions is continuously facilitated and shifted positively from −2.0 V (**L1**) to −1.69 V (**L4′**) with increasing OT chain length. Related to the reduction of parent *phen* ($E_{1/2}^{Red}$ = −2.62 V vs. Fc/Fc^+, THF), stabilization of the *phen*-centered radical anions due to coupling to the OT bridge is indicated.[13] A second reduction concomitant with the formation of dianions was noticed for all derivatives. **L1** and **L2** comprising shorter bridges revealed $E_{1/2}^{Red2}$ at −2.15 V, whereas for **L3, L4**, and **L4′** $E_{1/2}^{Red2}$ at −1.90, −2.01, and −2.23 V were detected. Finally, the electrochemical gap E_g^{CV} was determined from the energy differences of onset potentials and was found to decrease continuously from 2.71 eV for **L1** to 1.42 and 1.43 eV for the 4 T-ligands **L4** and **L4′**, respectively.

Complexation of (oligo)thiophene-bridged *bis*-phenanthroline ligands L1–L4 and L4′ with Cu(I)

ESI-HRMS spectra

In general, chelation of Cu(I) by ditopic ligands such as **L1**–**L4** and **L4′** should result in discrete mono- and dinuclear coordination products, but also mixtures of higher oligomeric or polymeric structures are possible. In this respect, formation of double-stranded dinuclear helicates from ditopic ligands is dominated by geometrical or electronic restrictions of the involved ligands, but also by external parameters such as concentration or solvents.[19,40] In order to promote selective formation of complexes with the dinuclear configuration **Cu_2L_2**, we applied an uniform protocol, in which 5×10^{-3} M solutions of the respective ligands **L1**–**L4** and **L4′** in DMF were reacted with equimolar solutions of $Cu(ACN)_4PF_6$ in acetonitrile (ACN). Subsequently, the volatile components were removed in order to prevent ligand displacement by the polar solvents. Solutions of the respective samples (DCM/ACN 1 : 1) were analyzed by positive ESI-HRMS, which is widely used for characterization of metal–organic supramolecular assemblies.[41,42] The detection of the ions by their respective mass-to-charge ratio enables the deduction of the stoichiometric composition of complex products by comparison of the peak spacing in the isotopic pattern, taking into account that for an n-valence ion the difference between every adjacent peak should be $1/n$.[43a,b]

The ESI-HRMS spectrum of the Cu(I) complex of **L1** revealed two pronounced signals at m/z = 1609.46 867 and m/z = 804.73 853 (Figure 2a). The latter value of the doubly charged ion corresponds to $[M/2]^{2+}$, that means $[Cu(\mathbf{L1})_2/2]^{2+}$, hence a mononuclear 1 : 2 metal-to-ligand stoichiometry was indicated. This result was corroborated by the isotopic pattern of the doubly charged ion which revealed a peak separation of 0.5 mass units (Figure 2b) and evidenced the exclusive formation of mononuclear $Cu(\mathbf{L1})_2$ assemblies.

The reaction of Cu(I) with 2 T-bridged bis-*phen* ligand **L2** resulted in a ESI-HRMS spectrum with a prominent signal at m/z = 918.19 952 (Figure S21). The m/z value corresponds to

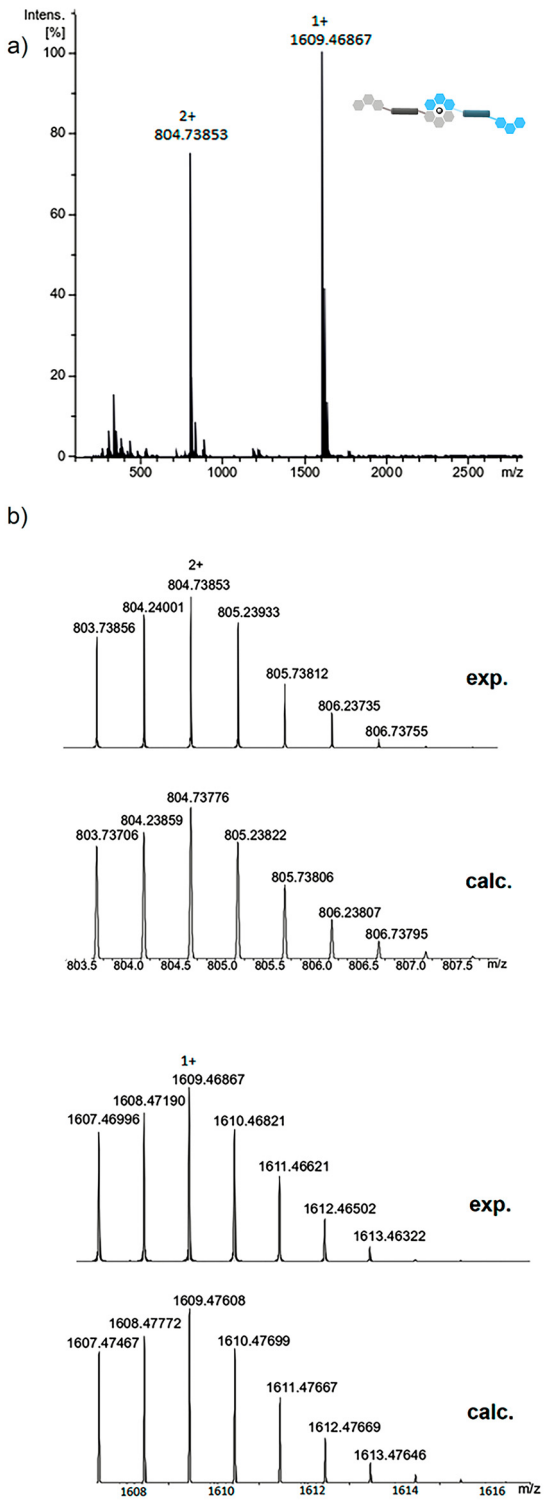

Figure 2 a) Positive ESI-HRMS of Cu(**L1**)$_2$ sprayed from a DCM/ACN solution. b) Comparison of calculated and measured isotopic patterns.

the calculated molecular mass of [Cu(**L2**)] or [Cu$_2$(**L2**)$_2$/2], which points to the formation of a 1 : 1 metal-to-ligand ratio. Nevertheless, in the isotopic mass pattern besides differences of 1.0 and 0.5 Da also a spacing of 0.33 Da was observed. This implied the presence of a $[M/2]^+$ fragment and various multiply charged species such as $[M/2]^{2+}$ and $[M/2]^{3+}$, respectively. Therefore, from the complexation reaction of **L2** with Cu(I), a mixture of Cu(**L2**) and higher oligomeric structures such as Cu$_2$(**L2**)$_2$ and Cu$_3$(**L2**)$_3$ becomes evident (Figure 3).

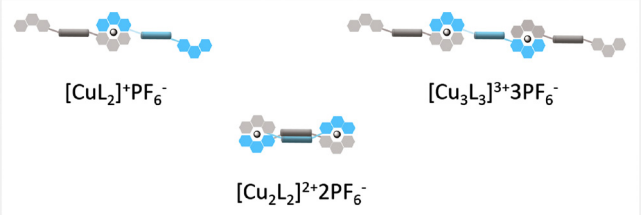

Figure 3 Possible coordination products from complexation of **L2** with Cu(I).

Similarly, the ESI-HRMS spectrum of 3 T-based derivative **L3** and Cu(I) revealed an intense signal at m/z = 999.17 730, which is in accordance with the calculated value of a Cu(**L3**) fragment and 1 : 1 metal-to-ligand stoichiometry. However, the resolved isotopic pattern of this peak indicates larger amounts of oligomeric byproducts besides the dimeric dinuclear structures Cu$_2$(**L3**)$_2$ (Figure S22).

Finally, for the stoichiometric composition of 4 T-based **L4**-Cu(I) complexes, ESI-HRMS revealed a pronounced signal of a doubly charged species $[M/2]^{2+}$ at m/z = 1082.66 921, which corresponds to [Cu$_2$(**L4**)$_2$/2] and a 1 : 1 metal-to-ligand stoichiometry (Figure 4). Analysis of the isotopic mass distribution confirmed the formation of a homoleptic dinuclear species Cu$_2$(**L4**)$_2$ because exclusively signals separated by 0.5 Dalton were observed. The absence of other peak distances and the accordance of the calculated and the measured isotopic pattern confirmed the exclusive formation of Cu$_2$(**L4**)$_2$ assemblies and ruled out the formation of oligomeric or polymeric assemblies as byproducts.

Apparently, the metal-templated assembly of ditopic *bis-phen* ligands into double-stranded helicates such as $[Cu_2\mathbf{L4}_2]^{2+}(PF_6^-)_2$ was favored by implementation of the longer 4 T-bridge between the two *phen* units. In that respect, we were interested to evaluate if the corresponding hexylated 4 T-based ligand **L4′** also coordinates with Cu(I) into homoleptic double-stranded dinuclear complexes. In the ESI-HRMS spectrum a prominent signal at m/z = 1251.35 641 was monitored which was assigned to [Cu$_2$(**L4′**)$_2$/2] as doubly charged $[M/2]^{2+}$ species (Figure S23). The isotopic mass distribution revealed most pronounced a peak separation of 0.5 Da, corroborating the formation of dinuclear dimeric helicates of Cu$_2$(**L4′**)$_2$. However,

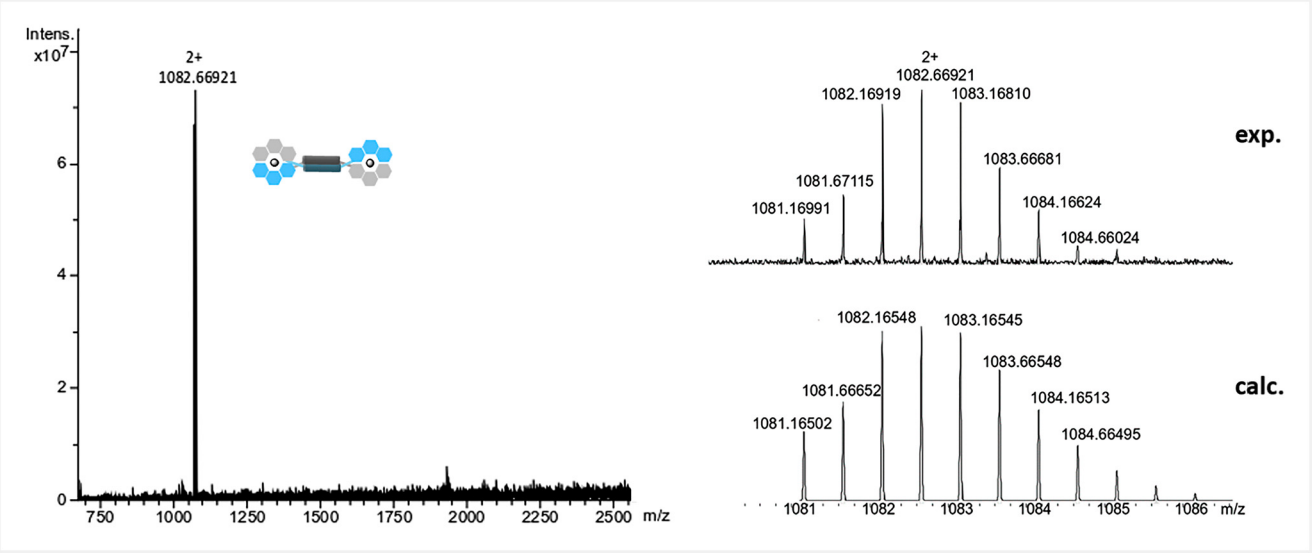

Figure 4 Left: positive ESI-HRMS of Cu_2(**L4**)$_2$ sprayed from DCM/ACN solution; right: comparison of calculated and measured isotopic patterns.

weak signals separated by 0.33 Da were also present in the mass spectrum indicating beginning of the formation of Cu_3(**L4′**)$_3$ assemblies.

^{1}H-NMR spectroscopy

For further structure elucidation, ^{1}H-NMR measurements of mononuclear [Cu(**L1**)$_2$]PF_6 in CD_2Cl_2 were accomplished. The corresponding spectrum showed an increased number of signals, which reflect that the C_2-symmetry observed for the free ligand **L1** was not retained (Figure 5, Figure S24).[44] Moreover, the signals of thiophene protons $H_{b,b'}$ at 7.71 ppm and $H_{a,a'}$ at 6.86 ppm, which coincide with the free ligand, were split and substantially upfield-shifted. Also the singlet of protons $H_{c,c'}$ at 8.12 ppm belonging to the bridging thiophene was significantly upfield-shifted to 7.20 ppm as a multiplet after coordination with Cu(I). The observed upfield shifts are characteristic for non-symmetric Cu(I)-complexes due to ring current effects and proximity of *phen* subunits with the thiophenes in the complex.[19]

^{1}H-NMR spectra of **L2**@Cu(I) and **L3**@Cu(I) showed non-resolvable signals most probably due to the presence of differently composed oligomeric or polymeric species (vide supra). Due to the low solubility of **L4**@Cu(I), non-assignable ^{1}H-NMR spectra were obtained as well. Nevertheless, in the ^{1}H-NMR spectrum of better soluble [Cu_2(**L4′**)$_2$]$(PF_6)_2$, a set of signals for the *phen* protons was observed, which were considerably downfield-shifted compared to those of the free ligand **L4′** (Figure S25). The broadening of these signals is generally observed for intertwined structures, in particular for signals of protons, which are located in close proximity to the crossing points[19] and were ascribed to dynamic equilibria on the NMR time scale. The number of signals in the aromatic region for dinuclear [Cu_2(**L4′**)$_2$]$(PF_6)_2$ indicated a preserved C_2-symmetry within the assemblies.

Quantum chemical calculation for Cu(L1)$_2$ and Cu_2 (L4)$_2$

In order to get insight into the different modes of interaction and stability of the metal-templated assemblies, quantum chemical calculations based on density functional theory (DFT with the hybrid density functional B3LYP and the 6 G-31*(d,p) basis set) were performed for ligands **L1** and **L4**. In the first step, the most stable molecular geometries were optimized and frontier orbitals and dipole moments were determined (Figure S26). Thereafter, the hyperpotential surfaces for the metal-templated assembly of ligands **L1** and **L4** with one and two Cu-atoms were analyzed, respectively (Figure S27). Whereas no stabilization of dinuclear complex Cu_2(**L1**)$_2$ was obtained, mononuclear coordinated Cu(**L1**)$_2$ showed two stable geometries with a tweezer and a stretched form. The most stable stretched geometry is shown in Figure 6 (left). Close to the complexation center, thiophene rings and the coordinated *phen*-units undergo π–π stacking at distances between 0.36 and 0.38 nm contributing to the stabilization of the whole assembly. For the dinuclear coordination product Cu_2(**L4**)$_2$, energy-minimized calculated molecular geometries were computed and the optimized geometry revealed a structure, in which the *phens* in one ligand display an orthogonal position with respect to each other creating a pseudotetrahedral conformation site for Cu(I) centers (Figure 6, right). The thiophenes undergo *syn*/*syn*/*anti* conformations which allow for π–π stacking between the terminal thiophenes of the two bridges. The alkyl chains at the terminal thiophenes stretch

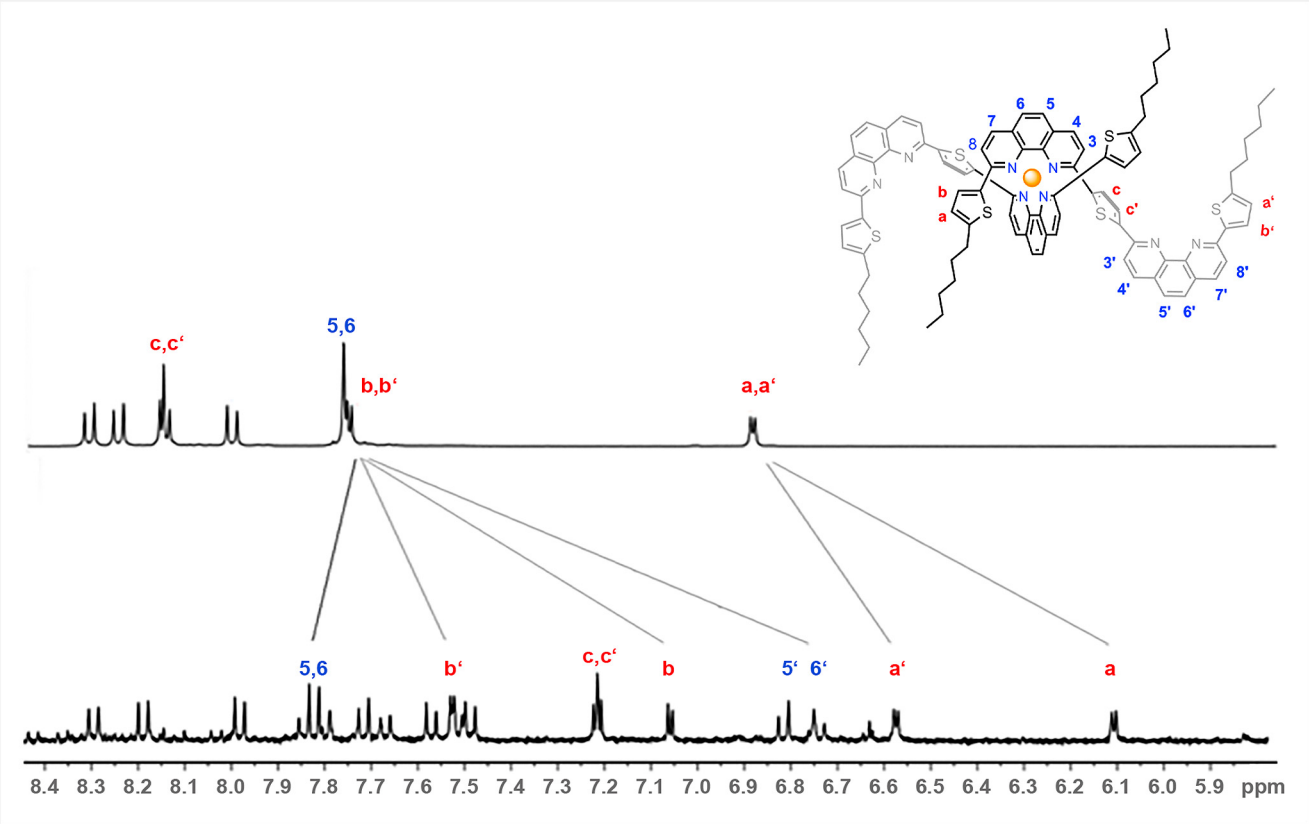

Figure 5 Aromatic region of ^{1}H-NMR spectra of **L1** (top) and $[Cu_1\mathbf{L1}_2]PF_6$ (bottom) in CD_2Cl_2.

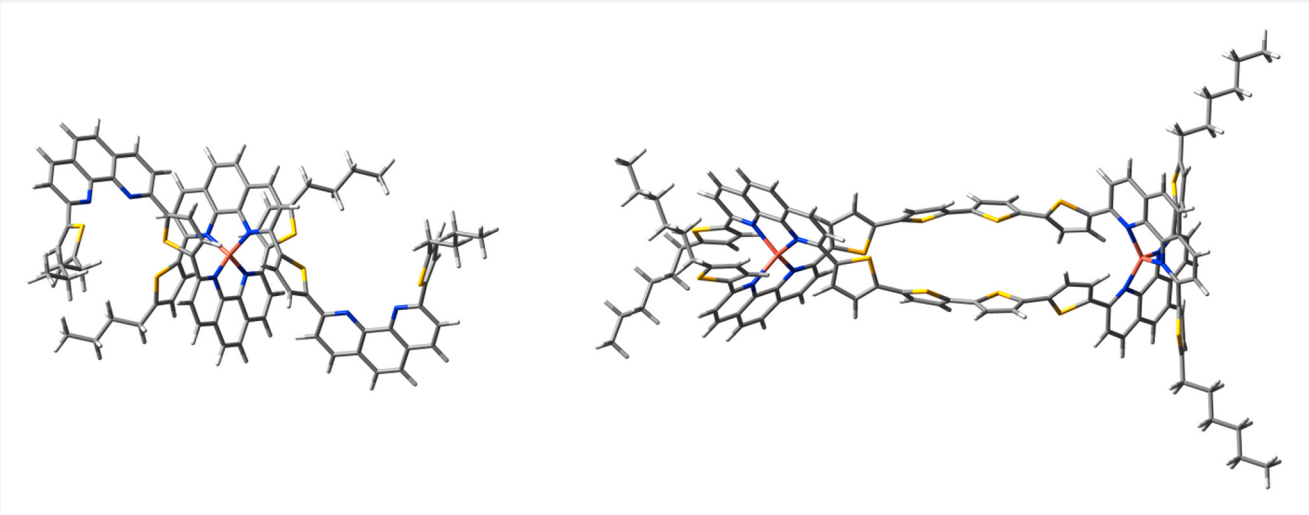

Figure 6 Calculated model of mononuclear $Cu(\mathbf{L1})_2$ (left) and dinuclear $Cu_2(\mathbf{L4})_2$ (right) assemblies. Atoms are color-labeled as follows: carbon grey, sulfur yellow, nitrogen blue, copper orange, and hydrogen white.

out of the complex centers avoiding perturbations in the complex geometry of the dinuclear complex.

The corresponding torsion angles between the *phen* units and adjacent thiophenes of the 4 T-segment were calculated to be 18° and 25°, still allowing π-conjugation between the

electron-rich thiophene and electron-deficient *phen* segments. The stability of the dimeric dinuclear Cu_2(**L4**)$_2$ was confirmed by the formation energy, which was 132.7 kJ/mol lower than the sum of the formation energies of the mononuclear components Cu(**L4**).

Optical properties of the Cu(I) complexes

In order to study the specific chelation properties of ligands **L1**–**L4** and **L4′** with Cu(I), 10^{-5} M solutions of the respective ligand were titrated with aliquots of a stock solution of $Cu(ACN)_4PF_6$ until equimolar concentrations of Cu(I) and ligand were reached. π-Stacking interactions of heteroaromatic N-donor ligands such as *phen* are known to promote the formation of Cu(I) chelates, hence for all titration experiments the less polar organic solvent DCM was employed.[40] Typically upon addition of Cu(I), a color change from yellow-orange to reddish was observed which is characteristic of the formation of Cu(I)-*phen* chelates.[41] The progress of the complexation reaction was monitored by UV-vis spectroscopy (Figure 7).

Successive addition of Cu (I) to solutions of the free ligand **L1–L4** and **L4′** induced strong alterations of the absorption profiles. In all cases, the ligand-centered π–π* transition bands at 400–500 nm were perturbed and the signature bands of the free *phen*-units mostly disappeared.[45] Concomitantly, emergence of d–π* metal-to-ligand charge transfer transitions (MLCT) at low energies was detected indicating coordination of the transition metal and unambiguously corroborating complex formation (Figure 7, left column). Calculated difference absorption spectra (Figure 7, middle column) guide the eyes to the changes occurring in the spectra during titration. The maximum wavelength of the MLCT band progresses from 438 nm (**L1**), to 485 nm (**L2**), to 510 nm (**L3**), to 519 nm (**L4′**), and to 528 nm (**L4**), which correlates well with the increasing electronic delocalization in the ligand. The optical gaps decreased from 2.64 eV (**L1**) to 2.15 eV (**L4**) (Table 2). These values were in the expected range and coincide with reported values of related mononuclear Cu(I)*phen*$_2$ structures.[46] The analysis of the UV-vis spectra (Figure 7, left column) revealed the appearance of various isosbestic points, which imply a well-defined equilibrium between the free and complexed ligands. The increase in absorption intensity of the maximum wavelength of the MLCT bands plotted versus equivalents of added Cu (I) agreed to a 1 : 2 metal-to-ligand stoichiometry in the case of **L2** and **L4′** and varied slightly for the rest, most probably due to the lower extinction coefficient of the MLCT band for **L1, L3**, and **L4**. In all cases, the complex formation was fitted as an exponential with a monomolecular limited growth function (Figure 7, right column). The stoichiometric composition of Cu(**L1**)$_2$ and Cu(**L2**)$_2$ was further supported by subsequently performed mass analyses, which exclusively revealed mononuclear homoleptic structures. The association constants (log K_a) for the complex formation were calculated from the fitted curve and gave values between 4.75 for Cu(**L1**)$_2$ and 5.75 for Cu(**L2**)$_2$. The calculated affinity constants of 5.18, 5.16, and 4.37 for the Cu-complexes of **L3, L4**, and **L4′**, respectively, were lower than that of the Cu(**L2**)$_2$ assembly, nevertheless, all values were in the same order of magnitude as those of mononuclear Cu(*phen*)$_2$-complexes with steric demanding substituents in the 2,9-position.[47] In both cases, the attenuation of the growth was shifted to higher values which indicated the formation of several dinuclear intermediates such as [**Cu$_2$(L3)**]$^{2+}$ and [**Cu$_2$(L4)**]$^{2+}$, in addition to the expected Cu(**L3**)$_2$, which then might further react to higher complexed structures.

Electrochemical properties of the Cu(I) complexes

Data of electrochemical properties of Cu(I)*phen*-complexes are scarce in the literature; therefore, we were interested to investigate the redox properties of our Cu(I)-ligand assemblies. Thus, as for the free ligands, oxidation and reduction potentials of the Cu(I)-complexes were investigated by CV and DPV in THF/$TBAPF_6$ (0.1 M) or DCM/$TBAPF_6$ (0.1 M) depending on their solubility in the electrolyte. Redox potentials are collected in Table 2 and were corrected against the internal reference $E_{1/2}^{Ox}$ (Fc/Fc^+). Exemplarily, the DPV of ditopic complex Cu_2(**L4′**)$_2$ is depicted in Figure 8 in compari-

Table 2 Optical and electrochemical data of equimolar complexed ligands **L1–L4** and **L4′** with Cu(I).

Cu(I) complex	λ_{max}^{abs} [nm]	λ_{max}^{abs} MLCT [nm]	λ_{onset} [nm]	E_g^{opt} [eV]	$E_{1/2}^{Ox1}$ [V]	$E_{1/2}^{Ox2}$ [V]	$E_{1/2}^{Ox3}$ [V]	$E_{1/2}^{Red1}$ [V]	$E_{1/2}^{Red2}$ [V]	E_g [eV]
Cu(**L1**)$_2$	302, *391*	438	469	2.64	**0.29**	–	–	**−1.62**	**−2.00**	1.91
Cu_2(**L2**)$_2$ [a]	326, 373, *459*	485	538	2.30	**0.36**	**0.64**	–	**−1.58**	**−1.83**	1.12
Cu_2(**L3**)$_2$ [a]	340, 442	510	545	2.27	**0.32**	**0.62**	**0.94**	**−1.34**	**−1.74**	1.18
Cu_2(**L4**)$_2$	360, 457	528	575	2.15	0.48	0.73	0.97	−1.59	−1.80	1.12
Cu_2(**L4′**)$_2$	360, 447	519	555	2.23	0.40	0.79	1.03	−1.45	−2.19	1.18

Absorption spectra of **L1**-Cu(I) to **L4**-Cu(I) and **L4′**-Cu(I) were measured in DCM. Italic values correspond to low-energy shoulder in the absorption spectra. Electrochemical data of **L1–L3** Cu(I) complexes were measured in THF (bold) and **L4–L4′** Cu(I) complexes were measured in DCM/tetrabutylammonium hexafluorophosphate (0.1 M), 100 mV · s^{-1}, r.t., potentials referenced against Fc/Fc^+. Half-wave potentials were determined via DPV. E_g^{CV} calculated by the difference of the first oxidation and reduction onset potentials. [a]Mixture with oligomeric and/or polymeric byproducts.

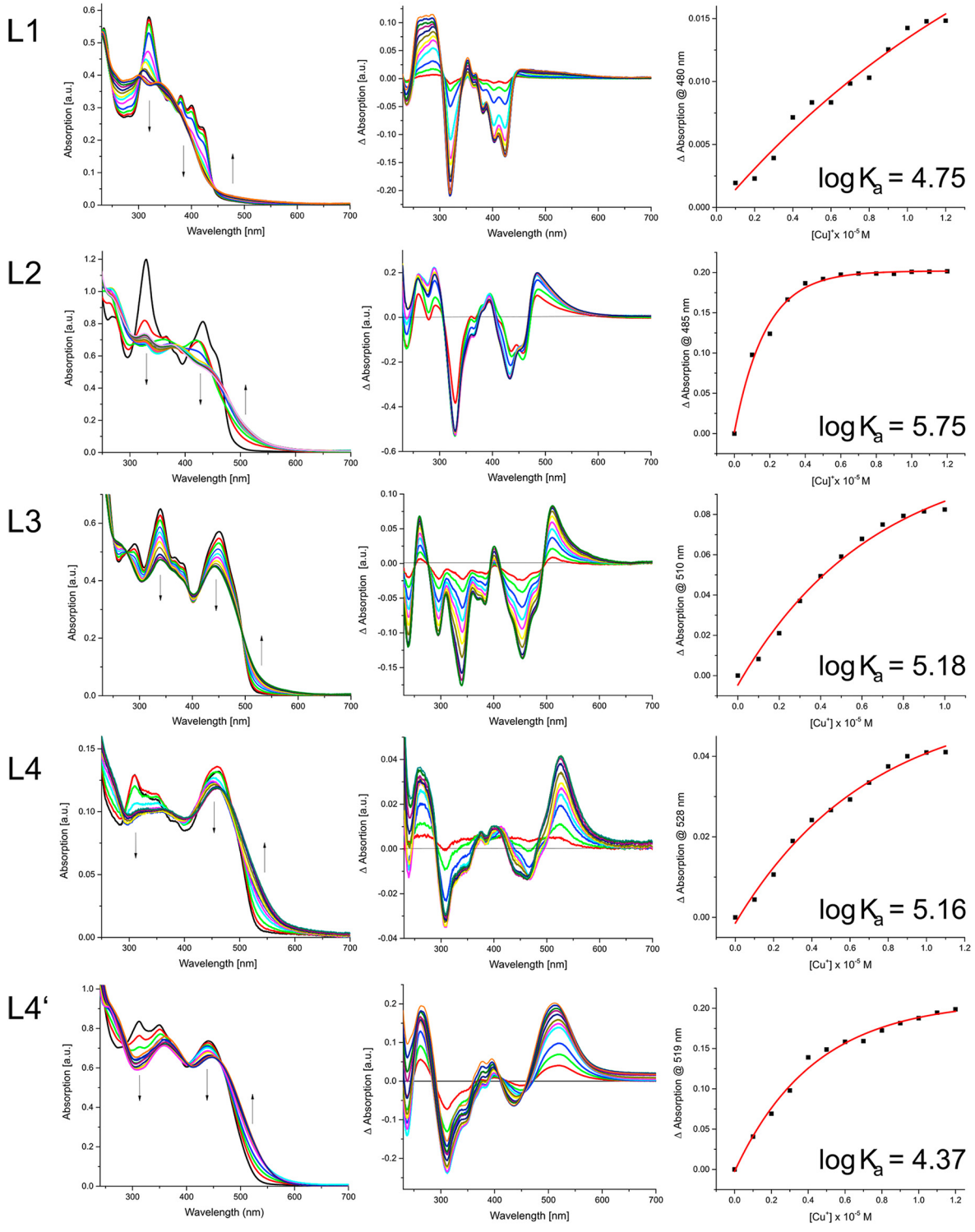

Figure 7 Spectroscopic results from the titration of ligands **L1**–**L4** and **L4′** with Cu(I) in DCM ($c = 10^{-5}$ M): UV-vis spectra (left column), difference spectra (middle column), and growth curve analysis for the low-energy emerging band (right column).

son to the DPV of the free ligand **L4′**. CVs/DPVs of the other Cu(I)*phen*-complexes are shown in Figures S28–S31.

In general, three different types of electrophoric subunits

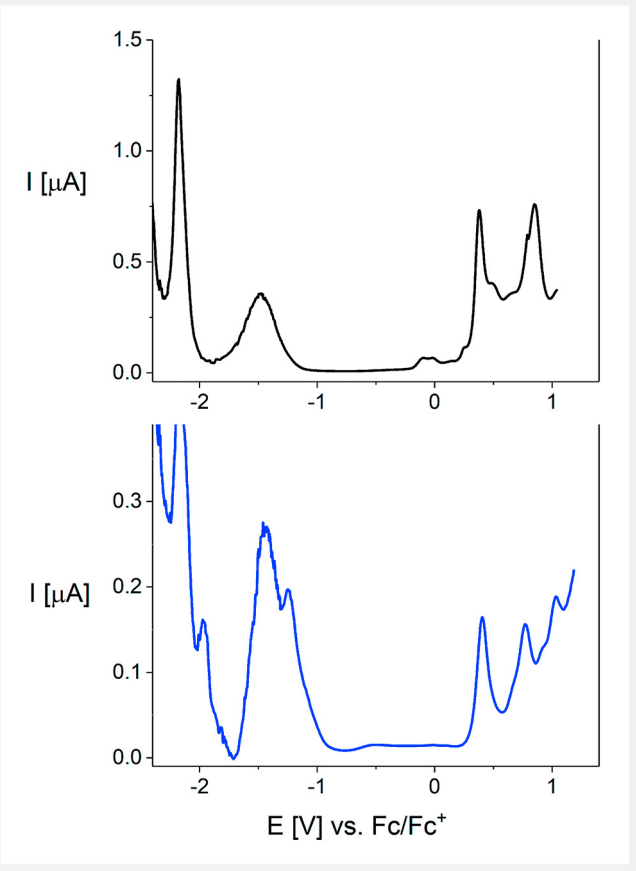

Figure 8 DPVs of ligand **L4′** (top) and Cu(I)*phen*-complex Cu_2(**L4′**)$_2$ (bottom) in DCM/$TBAPF_6$. Splittings of DPV waves we address to dimerization equilibria (see ref. 13).

are present in the various complexes: (1) Cu^+/Cu^{2+} redox couple and (2) the (oligo)thiophene bridges showed electrochemical response in the positive and (3) the *phen* moieties in the negative potential regime. As a complication for the assignment of the redox processes, the composition of the Cu(I)-complexes turned out to be different according to the HRMS measurements (Cu**L**$_2$ vs. Cu_2**L**$_2$) and therefore should influence the relative position of the potentials. Furthermore, for the ligands **L2** and **L3**, mixtures of Cu(I)-complexes were identified.

In the positive potential regime, we identify up to three oxidation processes for the Cu(I)-complexes depending on the length of the conjugated bridge instead of up to two for the free ligands. We address the first oxidation potential $E_{1/2}^{Ox1}$ to the Cu^+/Cu^{2+} redox couple, because it varies only limited from 0.29 V for Cu(**L1**)$_2$ to 0.48 V for Cu_2(**L4**)$_2$ and is comparable to the literature data on reported mononuclear 2,9-diarylated Cu(*phen*)$_2$ derivatives ($E_{1/2}^{CuI/II} \approx 0.21$–$0.25$ V vs. Fc/Fc^+)[46,48–50] and Cu(I)-catenates ($E_{1/2}^{CuI/II} = 0.35$ V vs. Fc/Fc^+).[51] We assign the continuing oxidation potentials, $E_{1/2}^{Ox2}$ and $E_{1/2}^{Ox3}$, to the first and second oxidation of the OT bridge under formation of radical cations and dications, respectively, which except for 2 T-based complexes **L2**@Cu(I) are located more positive in comparison to the free ligands due to the adjacent positive charge of Cu(II).

In the cathodic region of the CVs and DPVs of the Cu(I) *phen* complexes, typically two pronounced signals ($E_{1/2}^{Red1}$ from −1.41 V to −1.62 V; $E_{1/2}^{Red2}$ from −1.80 V to −2.19 V) are visible which correspond to the formation of radical anions and dianions of the *phen* segments (Table 2) and are anodically shifted compared to the free ligands (Table 1). Correspondingly, the HOMO/LUMO energy gaps are decreased with increasing length of the (oligo)thiophene bridge and range from 1.91 eV for Cu(**L1**)$_2$ to 1.12 eV for Cu_2(L4)$_2$.

The electrochemical investigation on our Cu(I)*phen* complexes elucidated the (expected) influence of the central Cu (I)-metal on the redox behavior of the electrophoric subunits in the complexes. Due to its electropositive character, reduction of the chelated *phen* ligands is eased and oxidation of the π-conjugated bridges is rather impeded.

Conclusions

A series of π-conjugated (oligo)thiophene-bridged bis(phenanthroline) ligands **L1**–**L4** and **L4′** was prepared in multistep synthesis by using transition metal-catalyzed aryl–aryl coupling reactions of halogenated phenanthrolines and metallated (oligo)thiophene units. The length of the bridge was systematically varied from thiophene to quaterthiophene which resulted in a clear influence on their optical and redox properties.

The complexation of the respective ligands with Cu(I) cations in metal–organic supramolecular assemblies was investigated and the synthesized dinuclear species represent rare examples of fully conjugated ditopic Cu(I)*phen*$_2$ complexes. Studies by ESI-HRMS revealed mono-coordinated products for (Cu(**L1**)$_2$) and dinuclear for Cu_2(**L2**)$_2$ to Cu_2(**L4′**)$_2$, but also mixtures containing higher oligomeric or polymeric structures were identified. Most interestingly, metal-templated assembly of ditopic *bis-phen* ligands into double-stranded helicates Cu_2(**L4**)$_2$ and Cu_2(**L4′**)$_2$ was favored by implementation of the longer quaterthiophene-bridge between the two *phen* units. ^{1}H-NMR spectra and quantum chemical calculations further corroborated the specific structures of the complexes. The study of the specific chelation properties of the ligands by titration with Cu(I) by absorption spectroscopy revealed the emergence of d–π* MLCTs. Resultant, corresponding association constants (log K_a) for the supramolecular complex formation were calculated. Electrochemical experiments with the Cu(I)*phen* complexes in comparison

to the metal-free ligands elucidated the influence of the central, electropositive Cu(I)-metal on the redox potentials of the subunits. These general insights into ditopic ligands, which form π-conjugated double-stranded helicates, should provide useful knowledge for the molecular design of Cu(I/II)-based redox mediators or catalysts, but should be also useful for further synthesis of (conjugated) catenanes or trefoil knots.

Experimental Section

Materials

All commercially available chemicals were purchased from Sigma Aldrich, TCI Germany, VWR International, Fisher Scientific, Acros Organics, Carl-Roth GmbH & Co., or Alfa Aesar. All of them were used without further purification. Anhydrous solvents were dried prior to use on an MBraun SPS-800 system. NMR spectra were recorded in the designated solvent on a Bruker Avance 400 MHz spectrometer and the data are given in ppm values from the residual protons of deuterated solvents. Mass spectrometry data were obtained with a Bruker Daltonics equipped with a 7.0 T superconducting magnet and interfaced to an Apollo II Dual ESI/MALDI source. For details on instrumentation and detailed methods, please refer to the Supporting Information.

Synthesis

Synthesis of 2-chloro-9-(5′-hexylthien-2′-yl)-1,10-phenanthroline **3**: a mixture of 2,9-dichloro-1,10-phenanthroline **2** (348.1 mg, 1.40 mmol), 2-hexyl-5-thienyl boronic acid pinacol ester **1** (559 mg, 1.9 mmol), and tetrakis(triphenylphosphane)palladium ($Pd[PPh_3]_4$) (231 mg, 0.20 mmol) were dissolved in dioxane (24 mL) under an argon atmosphere. Cs_2CO_3 (1.0 g, 3.5 mmol) dissolved in H_2O (3 mL) was added. The mixture was heated under reflux for 8 h. After cooling to room temperature (r.t.) and removal of the solvent under reduced pressure, the residue was re-dissolved in DCM (100 mL). The organic layer was washed with H_2O and dried over $MgSO_4$. After filtration of the solids and purification via column chromatography over silica gel using pentane → DCM as the eluent, pure phenanthroline **3** (361 mg, 0.95 mmol, 68%) was isolated as a yellow solid. Mp 114 °C; ^{1}H NMR ($CDCl_3$, 400 MHz) δ = 8.19 (d, *J* = 8.5 Hz, 1 H, H_7), 8.17 (d, *J* = 8.4 Hz, 1 H, H_3), 7.95 (d, *J* = 8.5 Hz, 1 H, H_8), 7.74 (m, *J* = 8.7 Hz, 2 H, H_5, H_6), 7.69 (d, *J* = 3.7 Hz, 1 H, $H_{3''}$), 7.60 (d, *J* = 8.4 Hz, 1 H, H_4), 6.87 (dt, *J* = 3.7 Hz, *J* = 0.9 Hz, 1 H, $H_{4''}$), 2.90 (t, *J* = 7.4 Hz, 2 H, α-CH_2), 1.78 (m, 2 H, β-CH_2), 1.34–1.44 (m, 6 H, γ-ε-CH_2), 0.91 (m, 3 H, CH_3) ppm; ^{13}C NMR ($CDCl_3$, 126 MHz) δ = 153.3, 151.4, 150.6, 145.8, 144.8, 142.3, 138.7, 136.6, 127.7, 127.5, 126.7, 126.3, 125.4, 124.8, 124.2, 119.3, 79.6, 78.2, 76.7, 76.6, 76.5, 76.4, 76.4, 76.5, 76.2, 76.0, 75.9, 75.7, 31.6, 30.6, 28.8, 22.6, 14.1 ppm; MS (CI): *m*/*z* = 381 ($M + H^+$), 345 ($M^+ - {}^{35}Cl$); HR-MS (FTICR-MALDI): *m*/*z* = [M + H$^+$] calcd. for $C_{22}H_{22}ClN_2S$: 381.1187, found: 381.11 825; *δm*/*m* = 1.18 ppm.

Synthesis of 2-(5-hexylthien-2-yl)-9-iodo-1,10-phenanthroline **8**: hydroiodic acid (57%, 9.0 mL) and hypophosphorous acid (50%, 0.4 mL) were stirred until decolorization occurred. Then, 89.9 mg (0.6 mmol) of sodium iodide and 119 mg (0.3 mmol) of 2-chloro-9-hexylthienyl-1,10-phenanthroline **3** were added. The mixture was heated to 93 °C for 1 h. Then the reaction was cooled with ice and treated with aq. NH_3 (25%) until the solution showed an alkaline reaction. After extraction with DCM and drying over Na_2SO_4, the crude product was concentrated under reduced pressure and purified by column chromatography over silica gel 60 (eluent: PE → DCM), from which phenanthroline **8** (126 mg, 0.27 mmol) was afforded (84% yield). Mp 160 °C; ^{1}H NMR ($CDCl_3$, 400 MHz) δ = 8.09 (d, *J* = 8.5 Hz, 1 H, H-3), 7.90 (d, *J* = 8.3 Hz, 1 H, H-7), 7.87 (d, *J* = 8.5 Hz, 1 H, H-4), 7.73 (d, *J* = 8.3 Hz, 1 H, H-8), 7.67 (d, *J* = 8.7 Hz, 1 H, H-5), 7.65 (d, *J* = 3.7 Hz, 1 H, H-3′), 7.56 (d, *J* = 8.7 Hz, 1 H, H-6), 6.85 (d, *J* = 3.7 Hz, 1 H, H-4′), 2.87 (t, 7.4 Hz, 2 H, α-CH_2), 1.74 (m, 2 H, β-CH_2) 1.24–1.54 (m, 6H, γ-ε-CH_2) 0.89 (m, 3H, CH_3) ppm; ^{13}C NMR ($CDCl_3$, 101 MHz, 2000 scans) 153.3, 150.6, 147.1, 144.8, 142.3, 136.9, 136.6, 134.2, 128.2, 127.3, 127.0, 126.4, 125.4, 125.1, 119.3, 119.3, 31.6, 30.6, 28.8, 22.6, 14.1 ppm. HR-MS (FTICR-MALDI): *m*/*z* [M + H]$^+$ calc. for $C_{22}H_{22}IN_2S$ *m*/*z* = 473.05 429, found: 473.05 426; *δm*/*m* = 0.06 ppm.

Synthesis of 9-chloro-2-(2′,2″-bithien-5″-yl)-1,10-phenanthroline **10**: 110 mg (0.44 mmol) of dichloro-1,10- phenanthroline **2**, 141 mg (0.48 mmol) of 2-(2,2′-bithien-5-yl)-4,4,5,5-tetramethyl-1,3,2-dioxa-borolane **9** and 43 mg (38 µmol) of $Pd[PPh_3]_4$ were dissolved in DME (20 mL, argon atmosphere). Subsequently, 400 mg (1.27 mmol) of $Ba(OH)_2$•$8H_2O$ in H_2O (4 mL) was added. The mixture was stirred at 80 °C for 16 h. After cooling to r.t., the reaction mixture was diluted with water and DCM. The phases were separated and the organic layer was dried over $MgSO_4$. After filtration and concentration under reduced pressure, the crude product was purified via column chromatography (silica gel 60, eluent PE: DCM (3 : 1) → DCM) from which pure phenanthroline **10** was provided in 66% yield. ^{1}H NMR (CD_2Cl_2, 400 MHz) δ = 8.22 (d, *J* = 8.5 Hz, 1 H, H-8), 8.19 (d, *J* = 8.4 Hz, 1 H, H-3), 7.99 (d, *J* = 8.5 Hz, 1 H, H-7), 7.76 (m, *J* = 8.7 Hz, 2 H, H-5,H-6), 7.69 (d, *J* = 3.9 Hz, 1 H, H-4″), 7.61 (d, *J* = 8.4 Hz, 1 H, H-4), 7.38 (dd, *J* = 3.6 Hz, 1.1 Hz, 1 H, H-4′), 7.29 (dd, *J* = 5.1 Hz, 1.1 Hz, 1 H, H-3′), 7.25 (d, *J* = 3.9 Hz, 1 H, H-3″), 7.07 (dd, *J* = 5.1 Hz, 1.5 Hz, 1 H, H-5′) ppm; ^{13}C-NMR (CD_2Cl_2, 101 MHz, 2000 scans) δ = 152.9, 151.4, 146.2, 145.5, 144.2, 141.3, 139.6, 137.8, 137.3, 128.7, 128.6, 127.4,

127.4, 125.8, 125.7, 125.2, 125.1, 124.7, 119.7 ppm. HR-MS (FTICR-MALDI): m/z [M$^+$] calc. for $C_{20}H_{11}ClN_2S_2$: 378.00522, found: 378.00268; $\delta m/m$ = 6.71 ppm.

Synthesis of 2-([2″,2‴-bithien]-5″-yl)-9-(5′-hexylthien-2′-yl)-1,10-phenanthroline **11**: 140 mg (0.36 mmol) of chloro derivative **10**, 141 mg (0.48 mmol) of 2-hexyl-thiophene-5-pinacol boronic acid ester **1**, 26 mg (0.02 mmol) of $Pd[PPh_3]_4$ and 120 µL of 1 M aq. Na_2CO_3 solution were dissolved in 20 mL of dioxane. After 16 h, the solvent was removed under reduced pressure and the crude residue was re-dissolved in DCM. The organic layer was washed with water, the layers were separated, and the organic phase was dried over $MgSO_4$. After filtration, the crude product was concentrated in vacuo and then purified by column chromatography over silica gel 60 using PE → DCM. Phenanthroline **11** (73 mg, 0.144 mmol) was isolated in 80% yield. ^{1}H NMR (THF-d_8, 400 MHz): δ = 8.24 (d, J = 8.4 Hz, 1 H, H-3), 8.21 (d, J = 8.4 Hz, 1 H, H-8), 8.04 (d, J = 8.4 Hz, 1 H, H-4), 7.99 (d, J = 8.4 Hz, 1 H, H-7), 7.83 (d, J = 3.9 Hz, 1 H, H-4″), 7.74 (d, J = 3.6 Hz, 1 H, H-4′), 7.70 (m, J = 1.0 Hz, 2 H, H-5,H-6), 7.39 (dd, J = 3.6 Hz, J = 1.1 Hz, 1 H, H-4‴), 7.37 (dd, J = 5.1 Hz, J = 1.1 Hz, 1 H, H-3‴), 7.29 (d, J = 3.9 Hz, 1 H, H-3″), 7.06 (d, J = 5.1 Hz, 1.5 Hz, 1 H, H-2‴), 6.87 (dt, J = 3.7 Hz, 0.9 Hz, 1 H, H-3′), 2.90 (t, 7.4 Hz, 2 H, α-CH_2, 1.78, m, 2 H, β-CH_2), 1.34–1.44 (m, 6H, γ-ε-CH_2) 0.9 (m, 3H, CH_3) ppm. ^{13}C NMR (THF-d_8, 101 MHz): 153.4, 152.7, 150.7, 147.1, 146.9, 146.4, 144.9, 141.5, 139.0, 137.3, 137.2, 129.0, 128.9, 128.7, 127.2, 126.7, 126.5, 126.1, 125.8, 125.4, 124.9, 119.1, 119.1, 68.1, 32.8, 31.6, 30.0, 26.0, 23.7, 14.6 ppm. HR-MS (FTICR-MALDI): m/z [M$^+$] calc. for $C_{30}H_{26}N_2S_3$: 510.1258, found 510.1251; $\delta m/m$ = 1.37 ppm.

Synthesis of 2-(5′-hexylthien-2′-yl)-9-(5‴-iodo-[2″,2‴-bithien]-5″-yl)-1,10-phenanthroline **12**: to a solution of 76 mg (0.15 mmol) of 2-([2,2′-bithien]-5-yl)-9-(5-hexylthien-2-yl)-1,10-phenanthroline **11** in 20 mL of a DCM/$CHCl_3$ mixture (1 : 1), 33.6 mg (0.15 mmol) of NIS and 0.5 mL of acetic acid were added. The mixture was allowed to stir at r.t. for 12 h under exclusion of UV light. Then, the reaction mixture was neutralized with aqueous ammonia, the phases were separated and the organic layer was washed with aqueous bisulfite solutions and dried over $MgSO_4$. After filtration, the solvent was removed under vacuum and the crude product was purified via column chromatography (silica gel 60, PE : DCM 1 : 1). The halogenated phenanthroline **12** (82.8 mg, 0.13 mmol) was isolated in 87% yield as a yellow solid. ^{1}H NMR ($CDCl_3$, 400 MHz): δ = 8.21 (d, J = 8.5 Hz, 1 H, H-8), 8.18 (d, J = 8.6 Hz, 1 H, H-3), 7,96 (d, J = 8.4 Hz, 1 H, H-7), 7,95 (d, J = 8.5 Hz, 1 H, H-4), 7.75 (d, J = 3.8 Hz, 1 H, H-3′), 7.70 (m, J = 2.0 Hz, 2 H, H-5,6), 7.69 (d, J = 3.6 Hz, 1 H, H-4″), 7.23 (d, J = 3.7 Hz, 1 H, H-3‴), 7.22 (d, J = 3.8 Hz, 1 H, H-4‴), 7.03 (d, J = 3.8 Hz, 1 H, H-3″), 6.89 (dt, J = 3.6 Hz, 1 H, H-4′), 2.90 (t, 7.4 Hz, 2 H, α-CH_2), 1.78 (m, 2 H, β-CH_2), 1.34–1.44 (m, 6 H, γ-ε-CH_2), 0.91 (m, 3H, CH_3) ppm. ^{13}C NMR ($CDCl_3$, 101 MHz, 2000 scans) δ = 152.9, 151.9, 150.4, 145.7, 145.5, 145.3, 143.9, 143.3, 139.2, 138.0, 136.8, 136.7, 128.0, 127.7, 126.2, 126.0, 125.7, 125.5, 125.5, 125.4, 125.1, 118.6, 118.5, 72.6, 31.8, 31.7, 30.8, 29.0, 22.8, 14.3 ppm. HR-MS (FTICR-MALDI): m/z [M + H]$^+$ calc. for $C_{30}H_{26}IN_2S_3$: 637.03028, found: 637.02947; $\delta m/m$ = 1.27 ppm.

Synthesis of 2′,5′-bis(9-(5″-hexylthien-2″-yl)-1,10-phenanthrolin-2-yl)thiophene **L1**: 152 mg (0.4 mmol) of 2-chloro-9-(5-hexylthien-2-yl)-1,10-phenanthroline **3** was dissolved in 35 mL of anhydrous toluene. 80 mg (0.2 mmol) of 2,5-bis(trimethylstannyl)thiophene **4** and 45 mg (40 µmol) of Pd$(PPh_3)_4$ were added and the mixture was degassed by freeze–pump–thaw method (3 cycles). After stirring at 80 °C for 14 h in a sealed tube, the mixture was allowed to cool down and water was added. The phases were separated and the organic phase was dried over $MgSO_4$. After filtration, the solvent was removed in vacuum and the crude product was purified via column chromatography over silica gel 60 using PE → DCM as the eluent. The orange solid was isolated in 78% yield (120 mg, 0.16 mmol). ^{1}H NMR (THF-d_8, 400 MHz) δ = 8.31 (d, J = 8.4 Hz, 2 H, H-3), 8.25 (d, J = 8.4 Hz, 2 H, H-8), 8.17 (d, J = 8.4 Hz, 2 H, H-4), 8.13 (s, 2 H, H-3′) 8.01 (d, J = 8.4 Hz, 2 H, H-7), 7.81 (d, J = 3.6 Hz, 2 H, H-4″), 7.75 (s, 4 H, H-5,5′,6,6′), 6.76 (d, J = 3.6 Hz, 1 H, H-3″), 2.90 (t, 7.4 Hz, 4 H, α-CH_2, 1.78, m, 4H, β-CH_2) 1.34–1.44 (m, 12H, γ-ε-CH_2), 0.91 (m, 6H, CH_3) ppm. ^{13}C NMR (THF-d_8, 101 MHz): 153.5, 153.1, 150.9, 149.4, 147.2, 147.1, 144.6, 147.4, 137.2, 129.2, 128.8, 128.1, 126.8, 126.7, 126.3, 126.0, 119.9, 119.1, 32.8, 32.5, 30.8, 30.1, 23.7, 14.6 ppm. HR-MS (FTICR-MALDI): m/z [M + H]$^+$ calc. for $C_{48}H_{44}N_4S_3$ = 773.28063, found 773.27952; $\delta m/m$ = 1.43 ppm.

Synthesis of 5,5′-bis[9-(5″-hexylthien-2″-yl)-1,10-phenanthrolin-2-yl][2,2′]bithiophene **L2**: 150 mg (0.4 mmol) of 2-chloro-9-(5-hexylthien-2-yl)-1,10-phenanthroline **3** was dissolved in 40 mL of anhydrous toluene. 93 mg (0.19 mmol) of 2,5-bis(trimethylstannyl)-2,2′-bithiophene **5** and 46 mg (40 µmol) of $Pd(PPh_3)_4$ were added and the mixture was degassed. After stirring for 14 h at 110 °C the mixture was allowed to cool and water was added. The phases were separated and the organic phase was dried over $MgSO_4$. After filtration, the solvent was removed in vacuum and the crude product was purified via column chromatography (silica gel 60, PE → DCM). After repeated column chromatography, the pure ligand **L2** was isolated in 65% yield (105 mg, 0.12 mmol). ^{1}H NMR (THF-d_8, 400 MHz): δ = 8.29 (d, J = 8.4 Hz, 2 H, H-3), 8.24 (d, J = 8.3 Hz, 2 H, H-8), 8.11 (d, J = 8.3 Hz, 2 H, H-4), 8.01 (d, J = 8.4 Hz, 2 H, H-7), 7.92 (d, J = 3.8 Hz, 2 H, H_c), 7.76 (d, J = 3.7 Hz, 2 H, H_b), 7.74 (s, 4 H, H-5,6), 7.50 (d, J = 3.9 Hz, 2 H, H_d), 6.82 (d, J = 3.3 Hz, 2 H, H_a), 2.86 (t, 7.4 Hz, 4 H, α-CH_2), 1.78 (m, 4 H, β-CH_2), 1.20–

1.42 (m, 12 H, γ-ε-CH_2), 0.80 (m, 6 H, CH_3) ppm. ^{13}C NMR (THF-d_8, 101 MHz): 153.5, 152.7, 151.0, 147.1, 147.0, 147.0, 144.8, 142.0, 137.3, 137.2, 129.1, 128.8, 127.4, 126.2, 126.0, 125.8, 119.1, 32.8, 32.6, 31.9, 30.8, 26.0, 23.7, 14.6 ppm. HR-MS (FTICR-MALDI): m/z $[M]^+$ calc. for $C_{52}H_{46}N_4S_4$: 854.2605, found: 854.26017; $\delta m/m$ = 0.39 ppm.

Synthesis of 5,5″-bis[9-(5-hexylthien-2-yl)-1,10-phenanthrolin-2-yl]-2,2′:5′,2″-terthiophene **L3**: 45 mg (90 µmol) of phenanthroline **8** was dissolved in 25 mL of anhydrous toluene and 21 mg (36 µmol) of 2-trimethylstannyl-terthiophene and 10 mg (9 µmol) of $Pd(PPh_3)_4$ were added. The mixture was degassed and subsequently allowed to stir for 4 h at 110 °C. After cooling, the crude mixture was treated with water, the layers were separated and the organic phase was dried over $MgSO_4$. The solvent was removed under reduced pressure. Subsequent purification via column chromatography (silica gel, eluent hexane → DCM) provided ligand **L3** (155 mg, 0.26 µmol) in 71% yield. ^{1}H NMR (400 MHz, THF-d_8): δ = 8.30 (d, J = 8.4 Hz, 2 H, H-3), 8.26 (d, J = 8.4 Hz, 2 H, H-8), 8.11 (d, J = 8.4 Hz, 2 H, H-4), 8.02 (d, J = 8.5 Hz, 2 H, H-7), 7.90 (d, 2 H, H_{th3}), 7.78 (d, J = 3.7 Hz, 2 H, $H_{3''}$), 7.75 (s, 4 H, H-5,6), 7.41 (s, 2 H, H_e), 7.39 (d, 2 H, $H_{2''}$) 6.88 (d, 2 H, H_{th4}), 2.96 (t, 7.4 Hz, 4 H, α-CH_2), 1.84 (m, 4 H, β-CH_2) 1.40–1.20 (m, 12 H, γ-ε-CH_2), 0.96–0.90 (m, 6 H, CH_3) ppm; ^{13}C NMR (THF-d_8, 101 MHz, RT) δ = 153.4, 152.6, 150.7, 147.0, 146.9, 146.8, 144.8, 141.0, 138.2, 137.3, 137.2, 129.0, 128.7, 127.4, 126.8, 126.6, 126.2, 126.2, 125.8, 125.7, 119.2, 119.1, 32.9, 32.7, 31.5, 30.0, 23.7, 14.7 ppm. HR-MS (FTICR-MALDI): m/z $[M]^+$ calc. for $C_{56}H_{48}N_4S_5$: = 936.2477, found: 936.24596; $\delta m/m$ = 1.86 ppm.

Synthesis of 5,5′′′-bis[9-(5-hexylthien-2-yl)-1,10-phenanthroline-2-yl]-(3,3′′′-dihexyl)-[2,2′:5′,2″:5″,2′′′]quaterthiophene **L4′**: 164 mg (0.44 mmol) of 2-chloro-9-(5-hexylthien-2-yl)-1,10-phenanthroline **3**, 83 mg (0.1 mmol) of bis-stannylated 3,3′′′-dihexyl[2,2′:5′,2″:5″,2′′′]quaterthiophene **6** and 46 mg (40 µmol) of $Pd[PPh_3]_4$ were dissolved in 28 mL of anhydrous toluene. The mixture was degassed by 3 freeze–pump–thaw cycles. After stirring at 100 °C for 16 h in a closed vial, the reaction mixture was allowed to cool and water was added. Then the phases were separated and the aqueous phase was repeatedly extracted with DCM. The combined organic phases were dried over $MgSO_4$. After filtration, the solvents were removed applying reduced pressure and the crude residue was purified by column chromatography (silica gel 60, PE → DCM → THF). Further purification via size exclusion chromatography (DCM) provided **L4′** (148 mg, 0.12 mmol) as an orange solid in 63% yield. ^{1}H NMR (THF-d_8, 400 MHz) δ = 8.30 (d, J = 8.4 Hz, 2 H, H-3), 8.26 (d, J = 8.4 Hz, 2 H, H-8), 8.11 (d, J = 8.4 Hz, 2 H, H-4), 8.02 (d, J = 8.5 Hz, 2 H, H-7), 7.90 (s, 2 H, H_e), 7.78 (d, J = 3.7 Hz, 2 H, H_b), 7.75 (m, 4 H, H-5,6), 7.33 (m, J = 3.8 Hz, 4 H, H_{cd}), 6.88 (dt, H_a), 2.96 (t, 7.4 Hz, 8 H, α-CH_2), 1.84 (m, 8 H, β-CH_2), 1.40–1.20 (m, 24H, γ-ε-CH_2), 0.96–0.90 (m, 2 × 6 H, CH_3) ppm; ^{13}C NMR (THF-d_8, 500 MHz) δ = 153.4, 152.6, 150.7, 147.1, 147.0, 145.3, 144.9, 141.6, 138.0, 137.3, 137.2, 137.1, 134.8, 129.8, 129.6, 129.0, 128.7, 127.8, 126.7, 126.6, 126.3, 126.2, 125.3, 119.1, 32.9, 32.8, 328, 31.6, 31.5, 30.8, 30.4, 30.0, 26.0, 23.7, 14.7 ppm; HR-MS (FTICR-MALDI): m/z $[M]^+$ calc. for $C_{72}H_{74}N_4S_6$: = 1186.4237, found: 1186.42352, $\delta m/m$ = 0.23 ppm.

Synthesis of 5,5′′′′-bis[9-(5-hexylthien-2-yl)-1,10-phenanthrolin-2-yl]-[2,2′:5′,2″:5″,2′′′]quaterthiophene **L4**: to a degassed solution of 72 mg (100 µmol) of phenanthroline **12** and 82 mg (800 µmol) of potassium acetate in 15 mL dioxane, 16.0 mg (20 µmol) of Pd(dppf) Cl_2•CH_2Cl_2 and 25.0 mg (100 µmol) of bis(pinacolato)diboron were added. After stirring for 16 hours at 80 °C, again 10 mg (40 µmol) of bis(pinacolato)diboron and 4 mg (5 µmol) of Pd(dppf) Cl_2•CH_2Cl_2 were added. The reaction mixture was allowed to react for further 16 h at 80 °C. After cooling to r. t., the mixture was diluted with water and repeatedly extracted with DCM and THF. The combined organic layers were dried over $MgSO_4$ and filtrated over a short column (silica gel 60, DCM). After removal of the solvent, **L4** (37 mg, 0.036 mmol) was isolated as an orange product in 71% yield. ^{1}H NMR (THF-d_8, 400 MHz) δ = 8.30 (d, J = 8.5 Hz, 2 H, H-3), 8.26 (d, J = 8.4 Hz, 2 H, H-8), 8.11 (d, J = 8.4 Hz, 2 H, H-4), 8.03 (d, J = 8.4 Hz, 2 H, H-7), 7.89 (d, J = 3.9 Hz, 2 H, H_c), 7.78 (d, J = 3.6 Hz, 2 H, H_b), 7.75 (m, 4 H, H-5,6), 7.39 (m, J = 3.9 Hz, 2 H, H_d), 7.37 (m, J = 3.9 Hz, 2 H, H_e), 7.31 (m, J = 3.2 Hz, 2 H, H_f), 6.91 (d, J = 3.6 Hz, 2 H, H_a), 2.98 (t, 7.4 Hz, 4 H, α-CH_2), 1.80–1.90 (m, 4 H, β-CH_2), 1.40–1.30 (m, 12 H, γ-ε-CH_2), 0.90 (m, 2 × CH_3) ppm; ^{13}C NMR (THF-d_8, 101 MHz): 152.3, 151.4, 149.5, 145.9, 143.7, 139.7, 136.9, 136.2, 136.1, 136.0, 127.9, 127.6, 126.2, 125.6, 125.4, 125.1, 125.1, 125.0, 124.7, 124.6, 124.6, 118.0, 118.0, 31.70, 31.6, 30.4, 28.9, 22.6, 13.5 ppm; HR-MS (FTICR-MALDI): m/z $[M]^+$ calc. for $C_{60}H_{50}N_4S_6$: 1018.2360, found: 1018.23555; $\delta m/m$ = 0.44 ppm.

Procedures

General procedure for the preparation of Cu(I)-helicates $\mathbf{Cu_2L_2(PF_6)_2}$: 4.68 µmol of the respective ligand in 0.1 mL DMF and 1.744 mg (4.68 µmol) of $Cu(CH_3CN)_4]PF_6$ in 0.1 mL ACN were mixed under inert conditions. After a reaction time of 16 h, the solvents were evaporated and residual copper was removed by rinsing with water. For ESI-HRMS spectra, 5×10^{-5} mol/L solutions in DCM/ACN 1 : 1 were prepared. $\mathbf{Cu(L1)_2PF_6}$, yield: 6.8 mg, 90.1%. $\mathbf{Cu_2(L4)_2 2PF_6}$, yield: 4.75 mg, 99.6%. $\mathbf{Cu_2(L4')_2 2PF_6}$ estimated yield > 95%.

Acknowledgements

We would like to acknowledge Christian Tontsch, Institute of Organic Chemistry I, Ulm University, for his support on ^{13}C-NMR measurements.

Supporting Information

Supporting Information is available online at https://doi.org/10.1055/a-1910-9165.

Conflict of Interest

The authors declare no conflict of interest.

References

(1) Fichou, D. *Handbook of Oligo- and Polythiophenes*, Wiley VCH: Weinheim, Germany, **1999**.
(2) Roncali, J.; Leriche P.; Cravino, A. *Adv. Mater.* **2007**, *19*, 2045.
(3) Mishra, A.; Ma, C.-Q.; Bäuerle, P. *Chem. Rev.* **2009**, *109,* 1141.
(4) Mishra, A.; Bäuerle, P. *Angew. Chem. Int. Ed.* **2012**, *51*, 2020.
(5) Scharber, M. C.; Mühlbacher, D.; Koppe, M.; Denk, P.; Waldauf, C.; Heeger, A. J.; Brabec, C. J. *Adv. Mater.* **2006**, *18*, 789.
(6) Accorsi, G.; Listorti, A.; Yoosaf, K.; Armaroli, N. *Chem. Soc. Rev.* **2009**, *38*, 1690.
(7) Omoto, K.; Tashiro, S.; Kuritani, M.; Shionoya, M. *J. Am. Chem. Soc.* **2014**, *136*, 17946.
(8) Ni, Z.; McDaniel, A. M.; Shores, M. P. *Chem. Sci.* **2010**, *1*, 615.
(9) Holder, E.; Langeveld, B. M. W.; Schubert, U. S. *Adv. Mater.* **2005**, *17*, 1109.
(10) Deng, Z.; Yang, X.; Yang, K.; Zhang, L.; Wang, H.; Wang, X.; Sun, L. *ACS Sustainable Chem. Eng.* **2021**, *9*, 5252.
(11) Saygili, Y.; Stojanovic, M.; Flores-Diaz, N.; Zakeeruddin, S. M.; Vlachopoulos, N.; Grätzel, M.; Hagfeldt, A. *Inorganics* **2019**, *17*, 30.
(12) (a) Kalsani, V.; Bodenstedt, H.; Fenske, D.; Schmittel, M. *Eur. J. Inorg. Chem.* **2005**, *2005*, 1841; (b) Kalsani, V.; Ammon, H.; Jäckel, F.; Rabe, J.; Schmittel, M. *Chem. Eur. J.* **2004**, *10*, 5481. (c) Schmittel, M. *Isr. J. Chem.* **2019**, *59*, 197.
(13) (a) Bäuerle, P.; Ammann, M.; Wilde, M.; Götz, G.; Mena-Osteritz, E.; Rang, A.; Schalley, C. *Angew. Chem. Int. Ed.* **2007**, *46*, 363. (b) Ammann, M.; Bäuerle, P. *Org. Biomol. Chem.* **2005**, *3*, 4143. (c) Götz, G.; Zhu, X.; Mishra, A.; Segura, J.-L.; Mena-Osteritz, E.; Bäuerle, P. *Chem. Eur. J.* **2015**, *21*, 7193.
(14) Collin, J.-P.; Dietrich-Buchecker, C. O.; Gavina, P.; Jimenez-Molero, M. C.; Sauvage, J. P. *Acc. Chem. Res.* **2001,** *34*, 477.
(15) Balzani, V.; Credi, A.; Raymo, F. M.; Stoddart, J. F. *Angew. Chem. Int. Ed.* **2000**, *39*, 3348.
(16) Vidal, P. L; Divisia-Blohorn, B.; Bidan, G.; Kern, J.-M.; Sauvage, J.-P.; Hazemann, J.-L. *Inorg. Chem.* **1999**, *38*, 4203.
(17) Kraus, T.; Budesinky, M.; Cvacka, J.; Sauvage, J.-P. *Angew. Chem. Int. Ed.* **2006**, *45*, 258.
(18) Dietrich-Buchecker, C. O.; Rapenne, G.; Sauvage, J.-P.; De Cian, A.; Fischer, J. *Chem. Eur. J.* **1999**, *5*, 1432.
(19) Piguet, C.; Bernardinelli, G.; Hopfgartner, G. *Chem. Rev.* **1997**, *97*, 2005.
(20) Beves, J. E.; Blight, B. A.; Campbell, C. J.; Leigh, D. A.; McBurney, R. T. *Angew. Chem. Int. Ed.* **2011**, *123*, 9428.
(21) Fielden, S. D. P.; Leigh, D. A.; Woltering, S. L. *Angew. Chem. Int. Ed.* **2017**, *56*, 11166.
(22) Velten, U.; Rehahn, M. *Chem. Commun.* **1996**, 2639.
(23) Zong, R.; Thummel, R. P. *J. Am. Chem. Soc.* **2005**, *127*, 12802.
(24) Zhong, R.; Wang, D.; Hammit, R.; Thummel, R. P. *J. Org. Chem.* **2006**, *71*, 167.
(25) Ruiz-Carretero, A.; Atoini, Y.; Han, T.; Operamolla, A.; Ippolito, S.; Valentini, C.; Carrara, S.; Sinn, S.; Prasetyanto, E. A.; Heiser, T.; Samori, P.; Farinola, G.; De Cola, L. *J. Mater. Chem. A* **2019**, *7*, 16777.
(26) Araki, K.; Endo, H.; Masuda, G.; Ogawa, T. *Chem. Eur. J.* **2004**, *10*, 3331.
(27) Balzani, V.; Barigelletti, F.; De Cola, L. *Top. Curr. Chem.* **1990**, *158*, 31.
(28) Papenfuss, T.M.; Mann, K. R. *Inorg. Chem.* **2001**, *40,* 6301.
(29) Cunningham, C. T.; Cunningham, K. L. H.; Michalec, J. F.; McMillin, D. R. *Inorg. Chem.* **1999**, *38*, 4388.
(30) Brandl, T.; Kerzig, C.; Le Pleux, L.; Prescimone, A.; Wenger, O. S.; Mayor, M. *Chem. Eur. J.* **2020**, *26*, 3119.
(31) Ochs, N. A. K.; Lewandowska, U.; Zajaczkowski, W.; Corra, S.; Reger, S.; Herdlitschka, A.; Schmid, S.; Pisula, W.; Müllen, K.; Bäuerle, P.; Wennemers, H. *Chem. Sci.* **2019**, *10*, 5391.
(32) Stone, D. A.; Hsu, L.; Stupp, S. I. *Soft Matter* **2009**, *5*, 1990.
(33) Ardoña, H. A. M.; Tovar, J. D. *Bioconjugate Chem.* **2015**, *26*, 2290.
(34) Leclere, P.; Surin, M.; Viville, P.; Lazzaroni, R.; Kilbinger, A. F. M.; Henze, O.; Feast, W. J.; Cavallini, M.; Biscarini, M.; Schenning, A. P. H. J; Meijer, E. W. *Chem. Mater.* **2004**, *16*, 4452.
(35) Haid, S.; Marszalek, M.; Mishra, A.; Wielopolski, M.; Teuscher, J.; Moser, J.-E.; Humphry-Baker, R.; Zakeeruddin, S. M.; Grätzel, M.; Bäuerle, P. *Adv. Funct. Mater.* **2012**, *22*, 1291.
(36) Linnell, R. H.; Kaczmarczyk, A. *J. Chem. Phys.* **1961**, *65*, 1196.
(37) Dietrich-Buchecker, C. O.; Sauvage, J.-P.; Kern, J.-M. *J. Am. Chem. Soc.* **1989**, *111*, 7791.
(38) Dietrich-Buchecker, C. O.; Sauvage, J. P.; Armaroli, N.; Ceroni, P.; Balzani, V. *New J. Chem.* **1996**, *20*, 801.
(39) Bäuerle, P.; Segelbacher, U.; Maier, A.; Mehring, M. *J. Am. Chem. Soc.* **1993**, *115*, 10217.
(40) Sigel, J.; Balakrishnan, R. M.; Häring, U. K. *J. Am. Chem. Soc.* **1985**, *107*, 5137
(41) Gütz, C.; Hovorka, R.; Struch, N.; Bunzen, J.; Eppler, G. M.; Qu, Z. W.; Grimme, S.; Topic, F.; Rissanen, K.; Cetina, M.; Engeser, M.; Lützen, A. *J. Am. Chem. Soc.* **2014**, *136*, 11830.
(42) Przybylski, M.; Glocker, M. O. *Angew. Chem. Int. Ed. Engl.* **1996**, *35*, 806.
(43) (a) McIndoe, J. S.; Viske, K. L. *J. Mass Spectrom.* **2019**, *54*, 446. (b) Gross, J. H. *Mass Spectrometry: A Textbook*, 3rd ed.; Springer: Cham, **2017**.
(44) Albrecht, M. *Chem. Rev.* **2001**, *101*, 3457.
(45) Kern, J.-M.; Sauvage, J.-P.; Weidmann, J.-L.; Armaroli, N.; Flamigni, L.; Ceroni, P.; Balzani, V. *Inorg. Chem.* **1997**, *36*, 5329.
(46) Vidal, P.-L; Divisia-Blohorn, B.; Bidan, G.; Hazemann, J.-L; Kern, J.-M.; Sauvage, J.-P. *Chem. Eur. J.* **2000**, *9,* 1663.
(47) Green, O.; Gandhi, B. A.; Burstyn J. N. *Inorg. Chem.* 2009, *48*, 5704.
(48) Leandri, V.; Pizzichetti, A. R. P.; Xu, B.; Franchi, D.; Zhang, W.; Benesperi, I.; Freitag, M.; Sun, L.; Kloo, L.; Gardner, J. M. *Inorg. Chem.*, **2019**, *58*, 12167.
(49) Armaroli, N.; Accorsi, G.; Gisselbrecht, J. P.; Gross, M.; Eckert, J.-F.; Nierengarten, J. F. *New J. Chem.* **2003**, *27*, 1470.

(50) Dietrich-Buchecker, C. O.; Nierengarten, J. F.; Sauvage, J. P.; Armaroli, N.; Balzani, V.; De Cola, L. *J. Am. Chem. Soc.* **1993**, *115*, 11237.
(51) Ammann, M. Ph.D. Thesis; University of Ulm: Germany, 2004.